Quantum dynamics of molecular multiphoton excitation in intense laser and static electric fields: Floquet theory, quasienergy spectra, and application to the HF molecule

ShihI Chu, James V. Tietz, and Krishna K. Datta

Citation: The Journal of Chemical Physics **77**, 2968 (1982); doi: 10.1063/1.444219

View online: http://dx.doi.org/10.1063/1.444219

View Table of Contents: http://scitation.aip.org/content/aip/journal/jcp/77/6?ver=pdfcov

Published by the AIP Publishing

Quantum dynamics of molecular multiphoton excitation in intense laser and static electric fields: Floquet theory, quasienergy spectra, and application to the HF molecule

Shih-I Chu,[a] James V. Tietz, and Krishna K. Datta

Department of Chemistry, University of Kansas, Lawrence, Kansas 66045
(Received 20 April 1982; accepted 20 May 1982)

The multiphoton excitation dynamics of vibration-rotation states in diatomic molecules in intense laser and static electric fields is investigated. The Floquet matrix method is used to calculate the quasienergy and multiphoton absorption spectra of the HF molecule as functions of field strengths and frequency. Nonlinear effects such as power broadening, dynamic Stark shift, Autler–Townes multiplet splitting, hole burning, and S-hump behaviors, etc., are observed and discussed in terms of quasienergy diagrams. Many of the salient features in the spectral line shapes may be qualitatively understood in terms of an analytical three-level model. The addition of a dc electric field removes the restriction of the rotational dipole selection rule and causes significant intermixing of the bare molecular vibrator states. Due to the greater number of strongly coupled nearby states in the dc field, nonlinear effects such as those mentioned above appear at a much lower ac field strength than they would in the absence of the dc field. The introduction of an external dc field, therefore, strongly enhances the multiphoton excitation probabilities and results in a much richer spectrum.

I. INTRODUCTION

The interaction of intense electromagnetic fields with multilevel atoms and molecules has been the subject of intensive theoretical and experimental investigations in recent years.[1–5] Important processes such as multiphoton ionization (MPI) of atoms,[2] collisionless multiphoton dissociation (MPD) of polyatomic molecules,[1–3] laser enhancement of atom(ion)–atom inelastic collisions,[4] and of chemical reactions,[5] just to mention a few, have been studied extensively. In this paper, we focus on the study of the quantum dynamics of collisionless molecular multiphoton excitation (MPE) in intense laser and dc electric fields.

Recently, it has been shown experimentally that the MPD reaction yield may be strongly enhanced by the introduction of additional external static electric[6(a)] or magnetic field.[6(b)] These external field effects are important in that they may help to improve our understanding of the detailed mechanism by which molecules subjected to coherent IR radiation can undergo unimolecular reaction. Further investigations along these external field effects may prove to be useful for improving the efficiency in future applications of isotopically selective MPD.

In this paper, we carry out a detailed study of the high-order nonlinear MPE dynamics of the vibration-rotational states of diatomic molecules in the presence of laser and static electric fields. As pointed out by van den Bergh *et al.*,[6] these external field effects occur predominately in the so-called region of the "discrete states". Thus, although MPD of diatomic molecules has not been observed experimentally, a study of the MPE dynamics in diatomics (which mimic the discrete regions of polyatomics) can provide useful insights about the underlying mechanism of MPD processes. Furthermore, the ability to incorporate the effects of static fields in the solution is important since a variety of other problems, such as anticrossing spectroscopy,[7] involve the applications of such fields to a level configuration interacting with an oscillating field.

In Sec. II, we outline the Floquet theory and quasienergy method appropriate for this problem. Application of the theory to single and multiphoton excitation of HF in the presence of laser and static electric fields is discussed in Sec. III. This is followed by a conclusion in Sec. IV.

II. FLOQUET THEORY AND QUASIENERGY METHOD FOR MOLECULAR MULTIPHOTON EXCITATION IN THE PRESENCE OF LASER AND STATIC ELECTRIC FIELDS

A. Summary of recent theoretical approaches using the Floquet theory

The use of the Floquet theory[8,9] for nonperturbative treatments of the multiphoton dynamics of atomic systems, involving periodic time-dependent Hamiltonians, has attracted considerable attention in the last few years. A detailed review of the theoretical treatments for the two-level system has been given recently by Dion and Hirschfelder.[9(a)] Moloney and Meath[9(b)] have developed a matching power-series matrix technique for N-level systems and have applied it to some finite-level model atomic systems. Chu and Reinhardt[10] have developed a non-Hermitian Floquet theory, the complex-dressed-state[10(a)] or the complex quasienergy[10(b)] approach, for nonperturbative treatment of intense field multiphoton ionization, incorporating the use of complex coordinate transformation[12] and L^2 continuum discretization. Extensions of the non-Hermitian Floquet theory to the study of Zeeman[11(a)] and Stark–Zeeman[11(a)] effects as well as to photoionization in the presence of laser and magnetic fields[11(b)] have also been developed.

The application of the Floquet theory to the molecular multiphoton excitation is relatively more recent. Moloney and Faisal[13] have extended the Floquet matrix approach of Shirley[8] to the computation of the multi-

[a]Alfred P. Sloan Foundation Fellow.

 0021-9606/82/182968-11$02.10

photon IR spectra of CO, incorporating the use of rotating wave approximation (RWA). Chu has discussed the quasivibrational energy method[14] and has used it in a semiclassical treatment of multiphoton enhancement of vibrational energy transfer. Wyatt and his coworkers[15] have discussed the Floquet characteristic exponent method[15(a)] and developed the Magnus approximation.[15(b)] They have applied their methods to the study of two-photon absorptions of several diatomic molecules. Cantrell, Letokhov, and Makarov[16] have reviewed the quasienergy or dressed-state approach and discussed the analytic solutions of several model systems. Finally, Chu has recently developed a *complex quasivibrational energy* method[17] for the treatment of intense field molecular photodissociation, using the complex coordinate transformation[12] and L^2 discretization of the vibrational continuum. This method is now being applied to the multiphoton dissociation of diatomic and triatomic molecules in intense laser fields.[18]

B. Floquet theory and quasienergy method for multiphoton excitation in the presence of sinusoidal and static electric fields

The Floquet theory can be also be extended to the problem of an N-level system interacting with sinusoidal and static electric fields. Moloney and Meath[19] have extended their matching power-series matrix technique to the study of the multiphoton spectra of some model atomic systems in the presence of strongly saturating oscillating and static fields. However, no detailed study of the multiphoton molecular excitation appears to exist. In the following, we outline the method we used in the current study.

Consider the vibrational-rotational motion of a heteronuclear diatomic molecule in the presence of a monochromatic electric field ϵ_{ac} of an IR laser as well as a static electric field ϵ_{dc}. The Schrödinger equation for the system in the electric-dipole approximation is

$$i\hbar \frac{\partial \Psi(\mathbf{r}, t)}{\partial t} = H(\mathbf{r}, t)\Psi(\mathbf{r}, t) , \tag{1}$$

where

$$H(\mathbf{r}, t) = H_0(\mathbf{r}) + V(\mathbf{r}, t) , \tag{2}$$

$$H_0(\mathbf{r}) = H^{(0)}(\mathbf{r}) - \mu(r) \cdot \epsilon_{dc} , \tag{3}$$

and

$$V(\mathbf{r}, t) = -\mu(r) \cdot \epsilon_{ac}(t) . \tag{4}$$

Here, $\mu(r)$ is the electric dipole moment of the diatom, $\epsilon_{ac}(t) = \epsilon_{ac}^0 \cos \omega t$, and $H^{(0)}$ is the Hamiltonian of the free molecule, with

$$[H^{(0)}(\mathbf{r}) - E_{vj}^{(0)}]\chi_{vjm_j}(\mathbf{r}) = 0 , \tag{5}$$

where $\chi_{vjm_j}(\mathbf{r})$ is the molecular vibration-rotational wave function, with (v, j, m_j) being the vibrational, rotational and angular momentum projection quantum number, respectively.

Without loss of generality, we shall take the molecular eigenstate to be the product of vibrational (Morse oscillator) $\xi_v(r)$ and spherical harmonics $Y_{jm_j}(\hat{r})$. Thus,

$$\chi_{vjm_j}(\mathbf{r} = r\theta\phi) = \xi_v(r)\, Y_{jm_j}(\hat{r}) , \tag{6}$$

and

$$E_{vj}^{(0)} = E_v(\text{Morse}) + E_j(\text{RR}) - \alpha_e j(j+1)(v+\tfrac{1}{2}) - \bar{D}_e[j(j+1)]^2 , \tag{7}$$

where the first two terms are the Morse oscillator and rigid rotor energies and the last two terms are due to inclusion of vibration-rotation interaction and centrifugal distortion, respectively. We further assume that $\epsilon_{ac} \parallel \epsilon_{dc} \parallel \hat{z}$, so that the electric dipole interactions have the form

$$\mu(r) \cdot \epsilon(\text{ac or dc}) = \mu(r)\, \epsilon^0(\text{ac or dc}) \cos\theta , \tag{8}$$

which is independent of the azimuthal angle ϕ. Thus, when fields are turned on, the angular momentum projection quantum number m_j remains a good quantum number (although v and j are no longer constants of motion).

Now that $H(\mathbf{r}, t) = H(\mathbf{r}, t+T)$, $T = 2\pi/\omega$, the Floquet theorem[8,9] admits the solution of Eq. (1) in the following form:

$$\Psi_\epsilon(\mathbf{r}, t) = \exp(-i\epsilon t)\, \phi_\epsilon(\mathbf{r}, t) , \tag{9}$$

where Ψ_ϵ is called the quasienergy state (QES) corresponding to the quasienergy ϵ (in this case the quasivibration-rotational energy ϵ_{vj}) and ϕ_ϵ is a periodic function of time, viz., $\phi_\epsilon(\mathbf{r}, t) = \phi_\epsilon(\mathbf{r}, t+T)$. Following the Floquet Hamiltonian method,[8-11,14] one can reduce the dynamic problem into an equivalent static problem. Thus, the QES Ψ_ϵ can be expanded into a Fourier series,

$$\Psi_{\epsilon_\alpha}(\mathbf{r}, t) = \exp(-i\epsilon_\alpha t) \sum_{n=-\infty}^{\infty} \exp(-in\omega t)\, \phi_{\epsilon_\alpha}^{(n)}(\mathbf{r}) , \tag{10}$$

where $\alpha = (vj)$ and $\phi_{\epsilon_\alpha}^{(n)}(\mathbf{r})$ is the quasienergy harmonics which is independent of time. To solve the quasienergy spectrum,[14] we further expand the quasienergy harmonics over an orthonormalized molecular-field basis $|\beta m\rangle$, where β runs over all (unperturbed) vibration-rotational states $\chi_{vjm_j}(\mathbf{r})$ (with m_j fixed) and m is a Fourier index which steps from $-\infty$ to $+\infty$:

$$\phi_{\epsilon_\alpha}^{(n)}(\mathbf{r}) \equiv |\lambda_{\alpha n}\rangle = \sum_\beta \sum_m |\beta m\rangle\langle \beta m|\lambda_{\alpha n}\rangle . \tag{11}$$

Substituting Eqs. (10) and (11) in Eq. (1), we obtain the following set of linear homogeneous equations (the Floquet matrix):

$$\sum_{\gamma k} \langle \alpha n|H_F|\gamma k\rangle F_{\gamma\beta}^k = \epsilon_\beta F_{\alpha\beta}^n , \tag{12}$$

where

$$\langle \alpha n|H_F|\gamma k\rangle = \langle \alpha|\mathcal{H}_F^{(n-k)}|\gamma\rangle + n\omega\delta_{\alpha\gamma}\delta_{kn} , \tag{13}$$

$$F_{\alpha\beta}^n \equiv \langle \alpha n|\lambda_{\beta 0}\rangle , \tag{14}$$

and

$$\mathcal{H}^{(m)} = T^{-1} \int_0^T dt \exp(im\omega t)\, H(\mathbf{r}, t)$$

is the mth Fourier harmonic of the Hamiltonian $H(\mathbf{r}, t)$. (Here, we use the Greek letters to denote the molecular states and Roman letters for Fourier components.) In deriving Eq. (12), use has been made of the periodic relation among the components of the eigenvector

$$\langle \alpha,\ n+p\,|\lambda_{\beta,m+p}\rangle = \langle \alpha n\,|\lambda_{\beta m}\rangle$$

and the fact that $|\lambda_{\alpha n}\rangle$ is a normalized eigenvector of H_F, the Floquet Hamiltonian, associated with the eigenvalue $\lambda_{\alpha n} \equiv \epsilon_\alpha + n\omega$. In Eq. (13), the nonvanishing Floquet matrix elements are

$$\langle \alpha\,|\,\mathcal{H}_F^{(0)}\,|\gamma\rangle = E_\alpha^{(0)}\,\delta_{\alpha\gamma} - \epsilon_{dc}\,\langle \alpha\,|\,\mu(r)\cos\theta\,|\gamma\rangle\ , \qquad (15)$$

and

$$\langle \alpha\,|\,\mathcal{H}_F^{(\pm 1)}\,|\gamma\rangle = -\,\epsilon_{ac}\,\langle \alpha\,|\,\mu(r)\cos\theta\,|\gamma\rangle/2\ . \qquad (16)$$

The quasivibration-rotational Floquet matrix so obtained possesses a block tridiagonal form as shown in Fig. 1. The determination of the vibration-rotational quasienergy and QES thus reduces to the solution of a time-independent Floquet matrix eigenproblem.[26] Figure 1 shows that $\hat{H}_F$ has a periodic structure with only the number of ω's in the diagonal elements varying from block to block. The structure endows the quasienergy eigenvalues and eigenvectors of $\hat{H}_F$ with periodic properties.

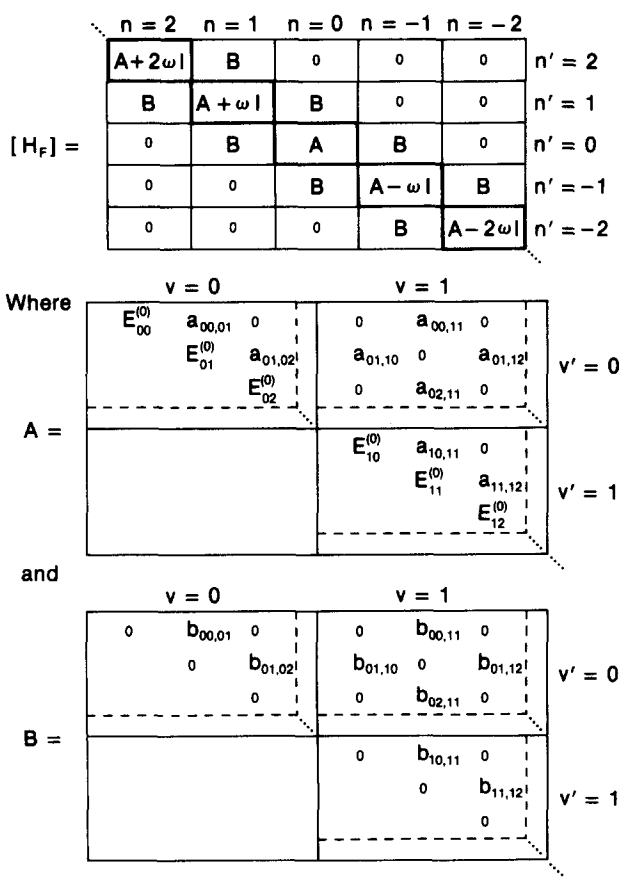

FIG. 1. Structure of the dc/ac Floquet Hamiltonian. The Hamiltonian is composed of the diagonal Floquet blocks, of type A, and off-diagonal blocks of type B. $E_{vj}^{(0)}$ are the unperturbed molecular energies and $a_{vj,v'j'}$ and $b_{vj,v'j'}$ are, respectively, the dc and ac coupling matrix elements.

TABLE I. HF molecular parameters.

A. Morse parameters[a]	
D =	6.125 eV
α =	$1.174\,1\,a_0^{-1}$
r_e =	$1.732\,9\,a_0$
M_H =	1.007 97 amu
M_F =	18.998 4 amu
B. Rotational constants and dipole moment[b]	
B_e =	20.4 cm^{-1}
α_e =	0.789 cm^{-1}
$\bar{D}_e$ =	2.2×10^{-3} cm^{-1}
μ_0 =	1.82 D
μ_1 =	$0.7876\ D\,a_0^{-1}$

[a]Reference 20(a). [b]Reference 20(b).

Finally, the time-averaged transition probability[26] from the initial state $\alpha(=vj)$ to the final state $\beta(=v'j')$ can be computed from the eigenvectors of the QES:

$$\bar{P}_{\alpha\to\beta}^{(m_j)} = \sum_k \sum_{\gamma l} |\langle \beta k\,|\lambda_{\gamma l}\rangle|^2 \cdot |\langle \lambda_{\gamma l}\,|\,\alpha 0\rangle|^2\ , \qquad (17)$$

where m_j is the rotational angular momentum projection quantum number which is conserved before and after multiphoton excitation.

III. MULTIPHOTON EXCITATION AND QUASIENERGY SPECTRA OF HF

In this section, we apply the quasienergy Floquet matrix method outlined in Sec. II to the study of multiphoton excitation (MPE) dynamics in HF in the presence of laser and static electric fields. In particular, we shall focus our discussion on the process

$$\mathrm{HF}(v=j=m_j=0) + n\hbar\omega + \text{dc field} \to \mathrm{HF}(v', j', m_j'=0)\ ,$$

which is sufficient to illustrate the salient features of the underlying mechanism in the MPE process.

A. Molecular parameters

We assume the HF molecule can be represented by a rotating Morse oscillator, so that

$$H^{(0)}(\mathbf{r}) = H^{\mathrm{Morse}}(r) + H^{\mathrm{RR}}(\hat{r})\ , \qquad (18)$$

where the Morse oscillator Hamiltonian is given by

$$H^{\mathrm{Morse}}(r) = -(\hbar^2/2\mu)\,d^2/dr^2 + D\{1-\exp[-\alpha(r-r_e)]\}^2\ , \qquad (19)$$

and H^{RR} is the rigid rotor Hamiltonian. The molecular dipole moment adopted has the following linear form:

$$\mu(r) = \mu_0 + \mu_1(r-r_e)\ , \qquad (20)$$

which is adequate for MPE of low-lying vibrational states. The molecular parameters used for HF are given in Table I.

B. Coupling matrix elements

The electric dipole coupling matrix elements given in Eqs. (15) and (16) are determined by

$$\langle \chi_{vjm_j}(r\theta\phi) \,|\, \mu(r)\cos\theta \,|\, \chi_{v'j'm'_j}(r\theta\phi)\rangle = \langle \xi_v(r) \,|\, \mu_0 + \mu_1(r-r_e) \,|\, \xi_{v'}(r)\rangle \cdot \langle Y_{jm_j}(\theta\phi) \,|\, \cos\theta \,|\, Y_{j'm'_j}(\theta\phi)\rangle$$

$$\equiv F_{\text{vib}}(v, v') \cdot F_{\text{rot}}(jm_j, j'm'_j) \,, \tag{21}$$

where the vibrational coupling matrix elements F_{vib} in the Morse oscillator basis $\xi_v(r)$ can be evaluated analytically using the formula derived by Gallas,[21] whereas the rotational coupling matrix elements can be reduced to the following familiar form:

$$F_{\text{rot}}(jm_j, j'm'_j) = \delta(m_j, m'_j) \cdot \begin{Bmatrix} \left[\dfrac{(j+1)^2 - m_j^2}{(2j+1)(2j+3)}\right]^{1/2}, & j' = j+1 \\ \left[\dfrac{j^2 - m_j^2}{(2j+1)(2j-1)}\right]^{1/2}, & j' = j-1 \end{Bmatrix} .$$

C. Numerical results

In this section, the dependence of the quasienergies and multiphoton time-averaged transition probabilities on the laser intensity I, laser frequency ω, and static field strength ϵ_{dc} will be studied for the HF molecule. This molecule has been the subject of several recent quantum mechanical studies of both single and multiple photon absorption[15,20] (in the absence of a static field). In this section, the response of HF is studied for medium strong ($I = 0.01$ TW/cm^2) and strong ($I = 1$ TW/cm^2) laser intensities. The dc field strengths used are $\epsilon_{dc} = 0$, 10^{-4}, and 5×10^{-4} a.u. (1 a.u. field strength = 5.14×10^9 V/cm). The frequency range varies from 3840 to 4060 cm^{-1}, and covers the most important one, two, and three photon transitions from the initial ($v = 0$, $j = 0$) state. For these computations on HF, the number of molecular vibrator basis states (which is the dimension of the matrix A in Fig. 1) used in 28, distributed (7, 7, 7, 7) (seven rotational states in $v = 0$, 1, 2, and 3 vibrational levels), which was found to be sufficient to obtain converged results for the highest field strengths studied here (i.e., $I = 1$ TW/cm^2 and $\epsilon_{dc} = 5\times10^{-4}$ a.u. or 2.57 MV/cm). Figures 2 and 3 show the converged MPE spectra ($v = j = 0 \rightarrow v'j'$) in HF for $I = 1$ and 0.01 TW/cm^2, respectively.

1. Rotating wave approximation (RWA)

Many of the authors involved in MPE calculations have employed the RWA.[13,22] This is to be expected since the RWA results in a significant savings of computer time. (In the Floquet matrix RWA calculation, the only diagonal blocks included are A, $A - \omega I$, $A - 2\omega I, \ldots$, etc., cf. Fig. 1.) In our study, it was found that at high ac field strength ($I = 1$ TW cm^2), the RWA broke down. For example, Fig. 2(d) shows that, at $I = 1$ TW/cm^2 and $\epsilon_{dc} = 2.57$ MV/cm, the RWA transition probability peaks are shifted in some cases by nearly 30 cm^{-1} with respect to the "exact" results [Fig. 2(c)]. Also evident from this figure are a number of line shape changes. These may be partially attributed to changes in the relative positions of the transitions, rather than an inherent quality of the RWA. At lower ac field strengths ($I = 0.01$ TW/cm^2), the RWA gives converged results [cf. Figs. 3(c) and 3(d)].

In this work, the RWA was used for the $I = 0.01$ TW/cm^2 case (Fig. 3), whereas the exact calculations were performed for the strong field case $I = 1$ TW/cm^2 (Fig. 2). Results were found to be converged to within 5% using seven Floquet blocks (i.e., $A \pm 3\omega I$, $A \pm 2\omega I$, $A \pm \omega I$, A) for the exact calculations and four Floquet blocks ($A - 3\omega I$, $A - 2\omega I$, $A - \omega I$, A) for the RWA calculations. All the calculations were carried out using the (7, 7, 7, 7) molecular vibrator basis.

2. Peak widths and mesh

The multiphoton spectra are generally much narrower than the one photon peaks. In our data, the mesh spacing along the frequency axis was adjusted to give accurate peak representations. In the weaker field case ($I = 0.01$ TW/cm^2), e.g., most of the three-photon peaks are so narrow that a mesh of 0.001 cm^{-1} is necessary to give the peak shape satisfactorily. (We ignore peaks with widths smaller than 10^{-3} cm^{-1}.) The mesh attained in our data is at least as good as that needed for comparison with experimental data.

One should note that the noncrucial portions of the data [those used mainly for convergence, i.e., Figs. 2(d), 3(d), and 5(a)] are of much coarser resolution and therefore miss many of the finer details of the better data. Since these data are replications, nothing is lost.

3. Observed phenomena

Many nonlinear effects are present in the data. Comparing Figs. 2 and 3, power broadening by the ac field is quite pronounced. Also evident in the data are dynamic Stark shifts. This effect is most pronounced for the three photon transitions. Several authors have reported Autler–Townes splitting under the influence of intense fields.[23] Previously, observed splitting has been primarily limited to the doublet case. We have observed multiplet splitting in much of our data. Figures 4(a) and 4(b) show that by using quasienergy graphs, virtually all of the features of the transition probability plots can be explained. For example, each of the peaks in the $0, 0 \rightarrow 2, 3$ multiplet [Figs. 4(c) and 4(d)] can be assigned a particular mechanism. We can use the major unperturbed component of the quasienergy states to identify the QES's involved in the transition mechanism.

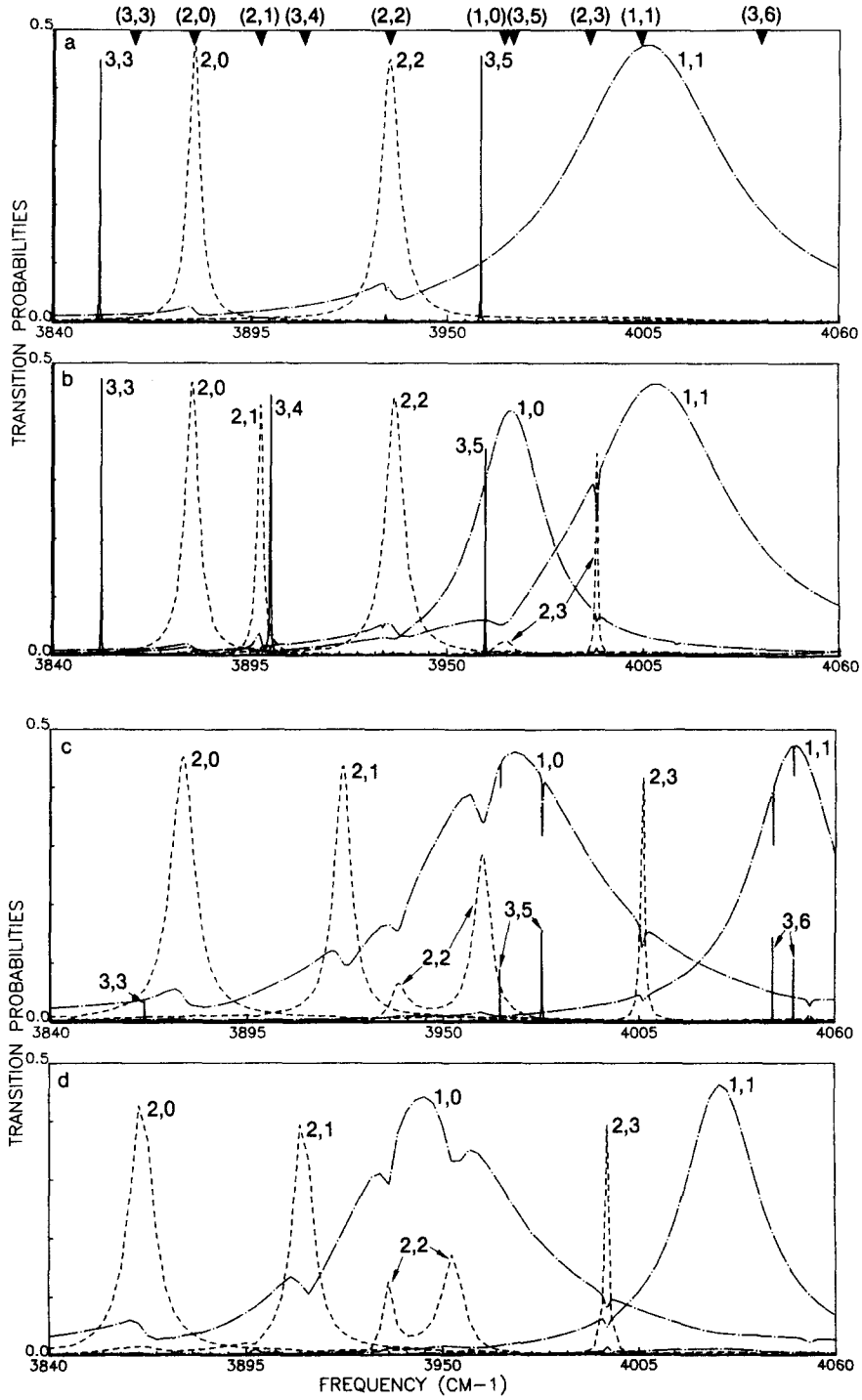

FIG. 2. Time-averaged MPE transition probabilities $\bar{P}_{00\to v'j'}$ for $\epsilon_{ac}=1.0$ TW/cm^2 and various dc strengths: (a) $\epsilon_{dc}=0.0$ a.u., (b) $\epsilon_{dc}=10^{-4}$ a.u., (c) $\epsilon_{dc}=5\times10^{-4}$ a.u., and (d) $\epsilon_{dc}=5\times10^{-4}$ a.u. (1 a.u. dc field strength $=5.14\times10^{-9}$ V/cm). Figures 2(a)–2(c) are exact numerical results obtained by including the seven Floquet cycles ($A\pm3\omega I$, $A\pm2\omega I$, $A\pm\omega I$, A) in Fig. 1, whereas Fig. 2(d) is the RWA results ($A-3\omega I$, $A-2\omega I$, $A-\omega I$, A) with coarser resolution. Significant shifts in the spectrum [cf. Fig. 2(d) with Fig. 2(c)] indicate the breakdown of the RWA at these high field strengths. In this figure, the line patterns are as follows: dot–dash lines indicate one photon peaks, dashed lines indicate two photon peaks, and solid lines show three photon peaks. The triangles on the top of (a) indicate the zero-field transition energies.

Starting at the low frequency side [Fig. 4(c) and 4(d)], the shape spike can be attributed to a 0, 0 – 3, 4 – 2, 3 sequence of QES transitions. The strong coupling between the 2, 3 and 3, 4 states makes this possible. The next peak arises from strong interactions between the 2, 2 and 2, 3 states and is due to a 0, 0 – 2, 2 – 2, 3 sequence. The peak at 3960 cm^{-1} is due to a mixture of the 0, 0 – 1, 1 – 2, 3 and 0, 0 – 0, 1 – 2, 3 sequences. The largest peak is due to the 0, 0 – 2, 3 transition. Lastly, the 0, 0 – 1, 0 – 2, 3 sequence is responsible for the peak at 4015 cm^{-1}. This type of rationalization can be used to explain the locations of many of the major and minor peaks in the spectra.

Other nonlinear features in the spectra seem to form a loosely related group. The phenomenon of hole burning has been widely reported[13,23(b)] and many examples may be found in these data. In some cases, however, the hole does not seem to be exactly matched in position or shape with the peak responsible for its presence [e.g., Fig. 2(c), the 0, 0 – 1, 0 – 2, 1 system]. In many instances, the situation is even more complicated with a region of enhancement side-by-side with the attenuation or hole [e.g., Fig. 2(a), the 0, 0 – 1, 1 – 2, 2 system]. In these cases, a characteristic S hump is observed.[13,24] If the situation is taken a step further, the enhancement becomes the major effect and little attenuation is noticed

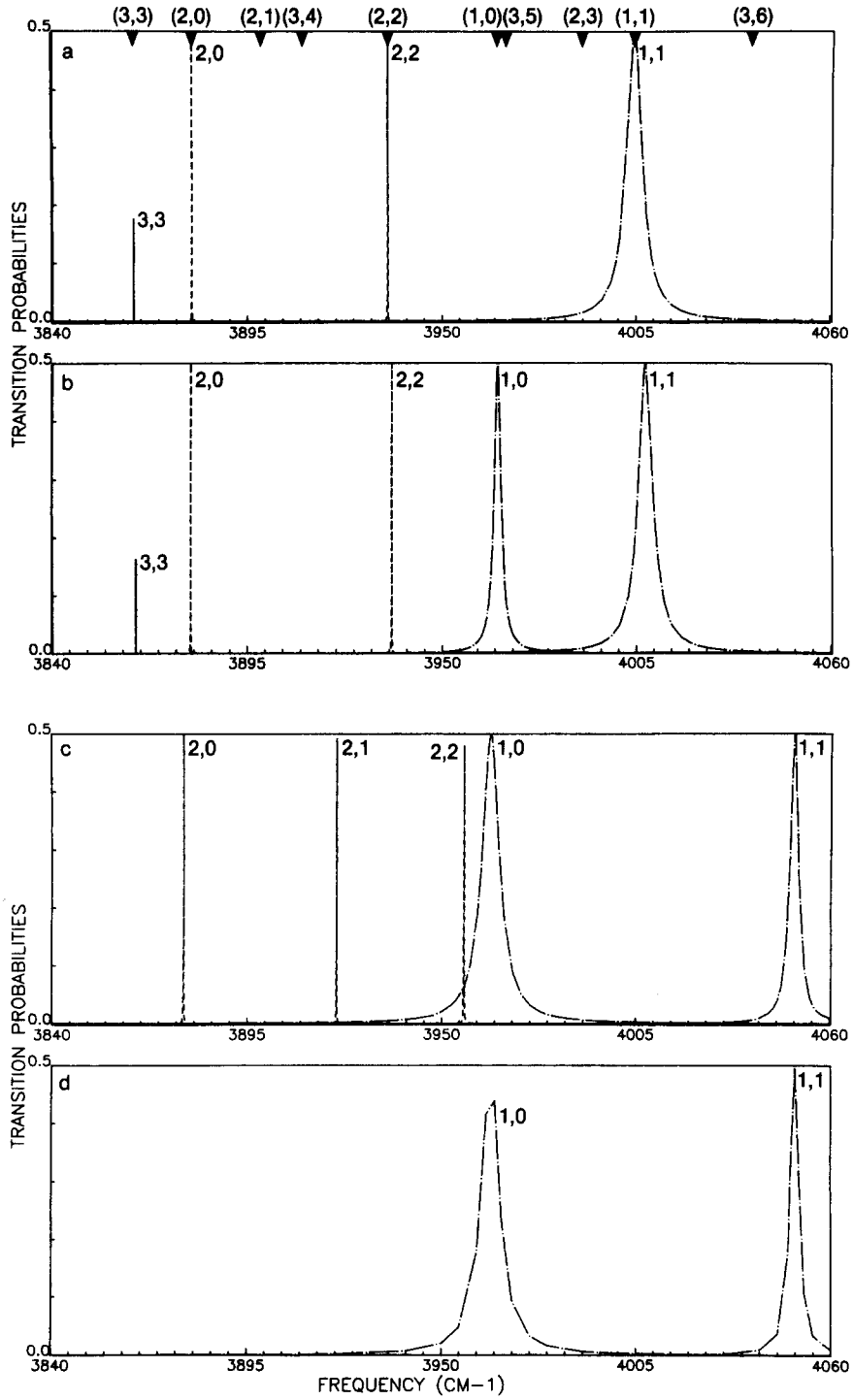

FIG. 3. Time-averaged MPE transition probabilities $\bar{P}_{00\to v'j'}$ for $\epsilon_{ac}=0.01$ TW/cm^2 and various dc strengths: (a) $\epsilon_{dc}=0.0$ a.u., (b) $\epsilon_{dc}=10^{-4}$ a.u., (c) $\epsilon_{dc}=5\times10^{-4}$ a.u., and (d) $\epsilon_{dc}=5\times10^{-4}$ a.u. Figures 3(a)–3(c) are the RWA data, whereas 3(d) is the exact data (with coarser resolution). Comparing Figs. 3(c) and 3(d) indicates that the RWA is approximately valid at this ac field strength. Line patterns are the same as in Fig. 2. Note that due to the extremely narrow linewidths ($<10^{-3}$ cm^{-1}), not all the three-photon peaks were located.

[e.g., Fig. 2(b), the 0, 0 − 1, 0 − 2, 1 system].

The hole burning, *S* hump, and enhancement behaviors are all similar effects stemming from the relative coupling strengths of the QES involved. These effects will be discussed in greater detail using a three-level analytical approximation below.

4. *dc effects*

As expected, the addition of a dc electric field removed the restrictions on transitions of the type $\Delta j \neq \pm 1$ (see Figs. 2 and 3). As the dc field is increased, significant intermixing of the bare states takes place. Individual transitions are generally broadened, though in some cases, the peaks actually get narrower (e.g., Fig. 2, the 0, 0 − 1, 1 peak). This indicates that the peak width is not directly dependent upon the dc field strength, but changes due to coupling between nearby quasienergy states.

Due to the greater number of strongly coupled nearby states in the dc field, nonlinear effects, such as those discussed above, appear at a much lower ac field strength than they would in the absence of the dc field. The addition of the dc field therefore results in a much

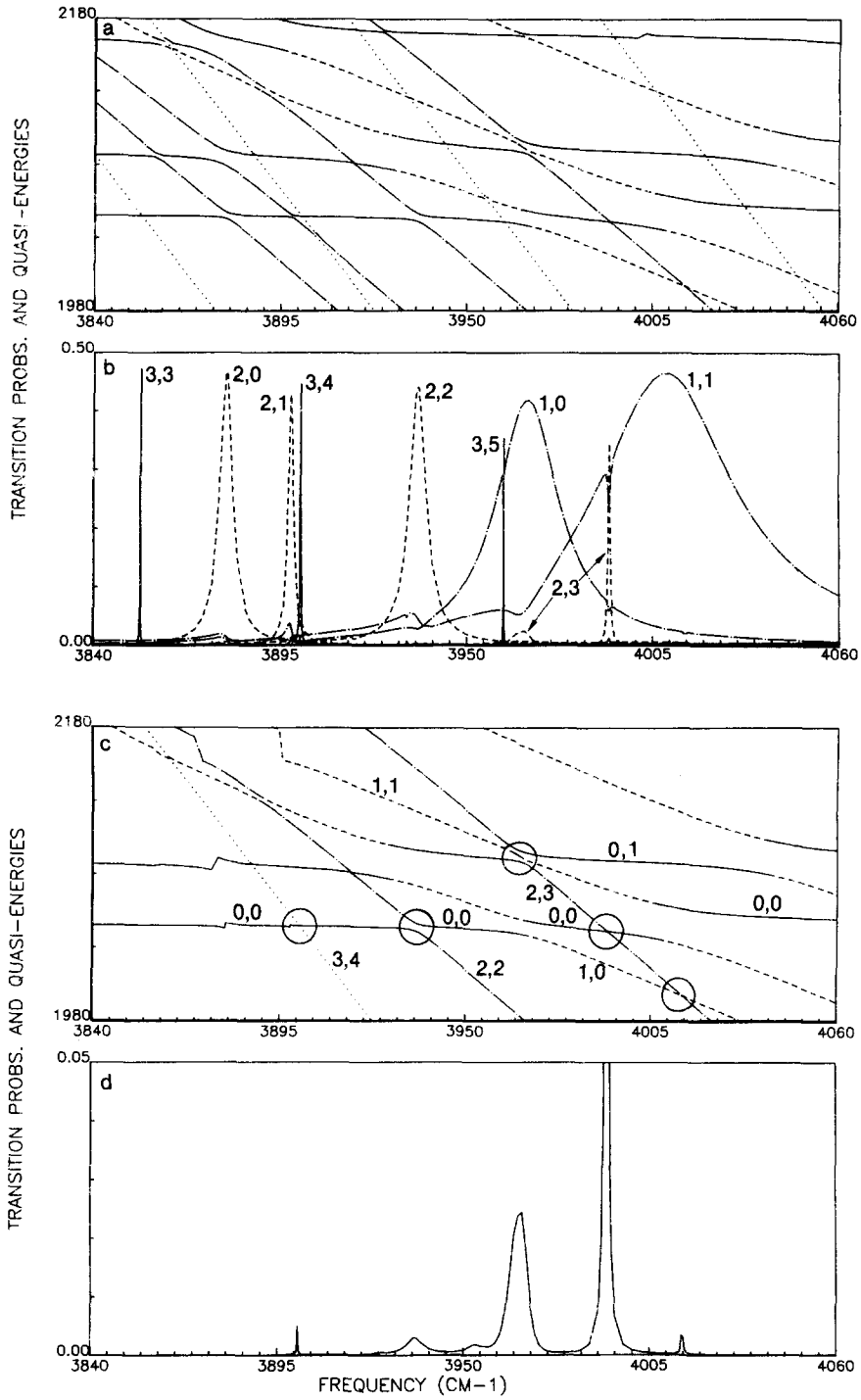

FIG. 4. Quasienergy plots (a) and (c) and exact time-averaged MPE transition probabilities (b) and (d) for the case of $\epsilon_{ac} = 1$ TW/cm^2 and $\epsilon_{dc} = 10^{-4}$ a.u. In (a) and (c), the quasienergy (in cm^{-1}) line patterns are as follows: solid lines refer to $v = 0$ states, dashed lines to $v = 1$ states, dot–dash lines to $v = 2$ states, and dotted lines to $v = 3$ states. Since $\epsilon_{dc} \neq 0$, all line encounters are avoided crossings (allowed transitions). In (b) and (d), the MPE line patterns are identical to those given in Figs. 2 and 3. Figures 4(a)–4(b) show that all the multiphoton absorption spectral features $\bar{P}_{00\to v'J'}$ can be approximately correlated with quasienergy level crossings and interactions. Figures 4(c)–4(d) show a more specific example of the correlation between $\bar{P}_{00\to 23}$ (multiplet structure) and the corresponding quasienergies. (Note ordinate magnification in d. Also the apparent discontinuities in c are antifacts of the selective display in quasienergies.)

richer spectrum than before. Since any one state is coupled to more and more of its neighbors, transitions involving that state can take place at many more frequencies due to a multiplicity of pathways available.

We note that van den Bergh *et al.*[6] have observed experimentally that the MPD yield of the polyatomic molecule first enhances linearly with increasing dc field strength and then reaches a plateau after certain ϵ_{dc}. Our HF data at the strong field cases (Fig. 2) indicate that the MPE enhancement effect induced by the dc field is still in the linearly rising region and has not reached the plateau region yet. Much stronger dc fields are required for diatomic molecules to attain the saturation of rotational angular momentum mixing.

D. Three-level approximation

Although the MPE spectra discussed in Sec. III C are rather complicated, many of the salient features of spectral line shapes may be qualitatively understood by means of three- or four-level analytic solutions. Appendix A gives a brief discussion of the three-level analytic solutions of QES and transition probabilities within the RWA. Figure 5 shows an example that the three-level approximation correctly mimics real be-

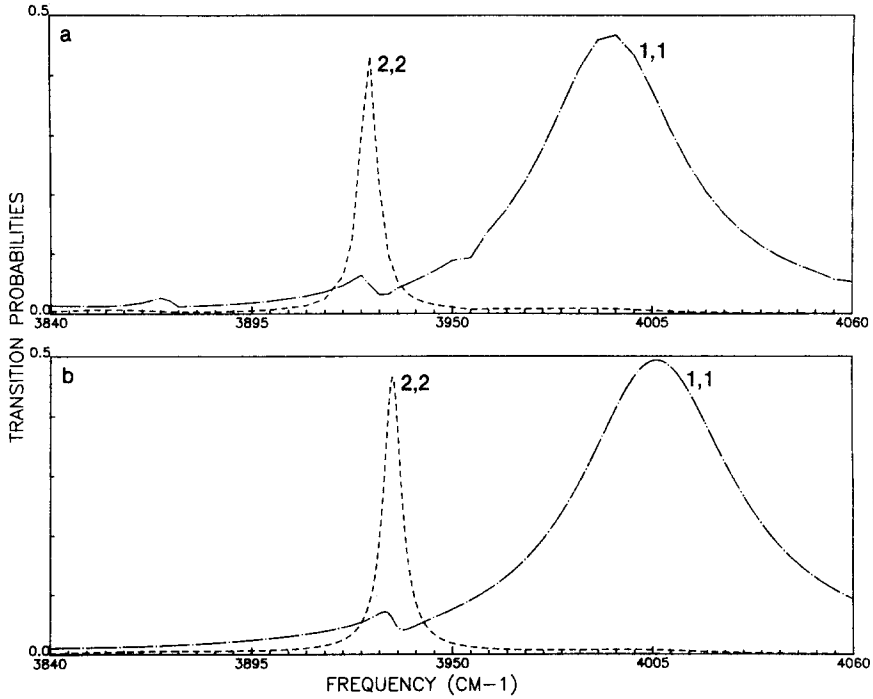

FIG. 5. Comparison of the exact RWA data [Fig. 5(a)] with the three-level approximation data [Fig. 5(b)] for the time-averaged MPE peaks $0,0 \rightarrow 1,1$ and $0,0 \rightarrow 2,2$ at $\epsilon_{ac} = 1$ TW/cm^2 and $\epsilon_{dc} = 0$.

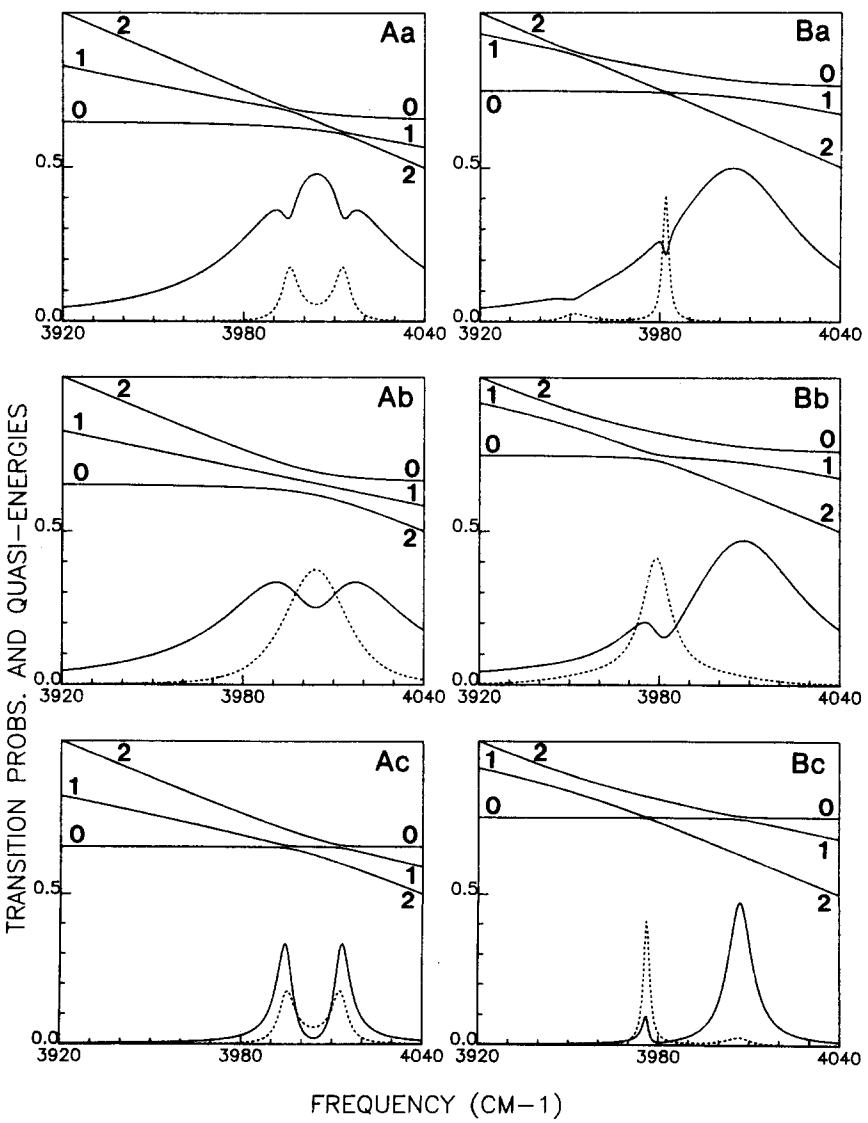

FIG. 6. Line shape analysis of MPE spectra using the three-level approximation. See Appendix B for detailed explanation.

havior within the RWA.

As mentioned before, some of the nonlinear features in intense field spectra can be explained by examining the relative couplings between the three levels in the approximation. Six of the nine possible interactions of three levels are diagrammed in Fig. 6. These are separated according to the relative coupling strengths of the three QES (labeled 0, 1, 2, respectively) involved and the amount of detuning in the system. The couplings between the upper two states (1 and 2) and the lower two states (0 and 1) can have the following relationships: $V_{01} > V_{12}$ (Fig. 6, row a), $V_{01} = V_{12}$ (row b), and $V_{01} < V_{12}$ (row c). The detunings can likewise be: $|E_2 - E_1| = |E_1 - E_0|$ (Fig. 6, column A), $|E_2 - E_1| < |E_1 - E_0|$ (column B), and $|E_2 - E_1| > |E_1 - E_0|$. The last case is not represented since it is less common in the systems examined here. The quasienergy diagrams for this case are the same as those in column B when viewed upside-down. Likewise, the features in the transition probability spectra will be switched high frequency to low and vice versa. A more detailed discussion of Fig. 6 is given in Appendix B.

By resorting to these six quasienergy diagrams, one can explain qualitatively many of the features found in intense field, multiphoton spectra. Likewise, by examining the features found experimentally, one can deduce qualitative information about the relative coupling strengths and detunings of the levels involved.

IV. CONCLUSIONS

At the present time, multiphoton dissociation (MPD) has not been observed in diatomic molecules. This is probably due to the low density of states near the ground state and the high anharmonicity interfering with the initial multiphoton excitation (MPE). As can be seen from the data presented here, MPE is extremely difficult for the HF molecule, even under the influence of very high fields. For a diatomic molecule, MPD can be expected to be observed only when the molecules are subjected to extremely strong fields.

Some authors have reported an enhancement in the MPD of polyatomic molecules when a static electric field is applied to the system.[6] It is presumed that this is due to a corresponding increase in the MPE for these systems. For a diatomic molecule like HF, the MPE is indeed increased by the addition of a dc field. The mechanism involved in the enhancement seems to be an increase in the richness of the spectrum. More transitions are allowed, many peaks are broadened, and many transitions are induced in regions where they normally would not appear.

ACKNOWLEDGMENTS

This research was supported in part by the United States Department of Energy, Division of Chemical Sciences, under contract No. DE-ACO2-80ER10748 and by the Alfred P. Sloan Foundation. Acknowledgment is also made to the Donors of the Petroleum Research Fund, administered by the American Chemical Society, for partial support of this work. We are grateful to the United Telecom Computing Group (Kansas City) for generous support of the CRAY computer time.

APPENDIX A: QUASIENERGIES AND DYNAMICS OF THREE-LEVEL SYSTEM

As is well known, the three-level system is one of the most useful models in the study of resonance phenomena in atoms or molecules and has been extensively discussed in the literature.[25] In this Appendix, we outline the analytic solutions of the QES and transition probabilities for a three-quasivibrator-level system interacting with an oscillating field ϵ_{ac} with (or without) the presence of static field ϵ_{dc}. The three levels chosen can be either the unperturbed vibrators (in the case of $\epsilon_{dc} = 0$) or the dc-perturbed vibrators (obtained by the prediagonization of the dc-coupling matrix A in Fig. 1).

It is convenient to try to find a solution of the Schrödinger equation

$$i\hbar \frac{\partial \Psi}{\partial t} = \hat{H}_0 \Psi - (\mu \cdot \epsilon_{ac} \cos \omega t)\, \Psi \,, \tag{A1}$$

in the form of expansion using the stationary eigenfunctions of the time-independent Hamiltonian $\hat{H}_0$,

$$\Psi = \sum_n a_n(t)\, \psi_n \exp(-in\omega t) \,, \tag{A2}$$

where

$$\hat{H}_0 \psi_n = \hbar E_n \psi_n \tag{A3}$$

$$\hat{H}_0 = \hat{H}^{(0)} - \mu(r) \cdot \epsilon_{dc} \,, \tag{A4}$$

and $\hat{H}^{(0)}$ is the Hamiltonian of the free molecule.

Thus, ψ_n and E_n are the dc-perturbed wave function and energy, respectively in the case of $\epsilon_{dc} \neq 0$. The following discussions, however, also hold for the case of $\epsilon_{dc} = 0$.

Substituting Eq. (A2) into Eq. (A1) and using the RWA approximation, one arrives at the following coupled equations for the probability amplitudes:

$$da_n/dt + i(E_n - n\omega)\, a_n = (i\epsilon_{ac}/2\hbar)\left[\langle n|\, \hat{\mu}\, |n-1\rangle a_{n-1} + \langle n|\, \hat{\mu}\, |n+1\rangle a_{n+1}\right] . \tag{A5}$$

When the field amplitude ϵ_{ac} is constant, the linearly independent solutions of Eq. (A5) may be written in the form

$$a_n(t) = P_n \exp(-i\lambda t) \,, \tag{A6}$$

where P_n is independent of time and λ is the eigenvalue (quasienergy) of the following system of time-independent linear equations

$$(E_n - n\omega - \lambda)\, P_n = (\epsilon_{ac}/2\hbar)\left[\langle n|\, \hat{\mu}\, |n-1\rangle P_{n-1} + \langle n|\, \hat{\mu}\, |n+1\rangle P_{n+1}\right] . \tag{A7}$$

The solution of Eq. (A1) becomes, in terms of quasienergies,

$$\Psi(\lambda) = \exp(-i\lambda t) \sum_n P_n(\lambda)\, \psi_n \exp(-in\omega t) \,, \tag{A8}$$

subjected to the following orthonormalization condition:

$$\sum_n P_n^*(\lambda_1)\, P_n(\lambda_2) = \delta_{\lambda_1 \lambda_2} \,. \tag{A9}$$

In the special case of three-level system (with $E_0 < E_1 < E_2$), the RWA linear equations (A7) become

$$\begin{aligned} -\lambda P_0 + V_{01} P_1 &= 0 , \\ V_{10} P_0 - (\lambda - \epsilon_{10}) P_1 + V_{12} P_2 &= 0 , \\ V_{21} P_1 - (\lambda - \epsilon_{20}) P_2 &= 0 , \end{aligned} \tag{A10}$$

where $\epsilon_{m0} = (E_m - E_0) - m\omega$ is the detuning and $V_{m,m+1}$ $V_{m+1,m} = (\epsilon_{ac}/2\hbar) \langle m | \hat{\mu} | m+1 \rangle$ is the Rabi frequency. Equation (A10) leads to the following equation for the quasienergy secular determinant:

$$\lambda^3 - (\epsilon_{20} + \epsilon_{10})\lambda^2 + (\epsilon_{10}\epsilon_{20} - |V_{01}|^2 - |V_{12}|^2)\lambda + \epsilon_{20}|V_{01}|^2 = 0 . \tag{A11}$$

The solutions for λ are

$$\begin{aligned} \lambda_0 &= 2Q^{1/2} \cos(\tfrac{1}{3}\theta) - \tfrac{1}{3}c_0 , \\ \lambda_1 &= 2Q^{1/2} \cos(\tfrac{1}{3}\theta + \tfrac{2}{3}\pi) - \tfrac{1}{3}c_0 , \\ \lambda_2 &= 2Q^{1/2} \cos(\tfrac{1}{3}\theta + \tfrac{4}{3}\pi) - \tfrac{1}{3}c_0 , \end{aligned} \tag{A12}$$

where

$$\begin{aligned} \cos\theta &= R \cdot Q^{-3/2} , \\ R &= (9c_0c_1 - 27c_2 - 2c_0^3)/54 , \\ Q &= (c_0^2 - 3c_1)/9 , \end{aligned}$$

and coefficients of the secular equation are

$$\begin{aligned} c_0 &= -(\epsilon_{20} + \epsilon_{10}) \\ c_1 &= (\epsilon_{10}\epsilon_{20} - |V_{01}|^2 - |V_{12}|^2) , \\ c_2 &= \epsilon_{20}|V_{01}|^2 . \end{aligned}$$

The probability that the system will be found in the state $|n\rangle$ at time t_2 if it was in the state $|m\rangle$ at time t_1 can be shown easily to be

$$P(n, t_2 | m, t_1) = \left| \sum_{\lambda} P_n(\lambda) P_m(\lambda) \exp[-i\lambda(t_2 - t_1)] \right|^2 , \tag{A13}$$

and the time-averaged transition probability is

$$\bar{P}(n|m) \equiv \bar{P}_{m\to n} = \sum_{\lambda} |P_n(\lambda) P_m(\lambda)|^2 , \tag{A14}$$

where the amplitude $P_n(\lambda)$ for the three-level system can be cast into closed analytic form and evaluated easily.

APPENDIX B: EXPLANATION OF FIGURE 6

Plotted in Fig. 6 are the transition probabilities between the lowest energy level and each of the upper levels of a three level model system. Transitions between the 0 and 1 levels are plotted with solid lines while the 0 – 2 transitions are dashed. The energy levels used to produce this graph were $E_0 = 0$ cm^{-1}, $E_1 = 4004$ cm^{-1}, and $E_2 = 8008$ cm^{-1} or 7958 cm^{-1} for columns A and B, respectively. Couplings between the states were arbitrarily picked to give informative graphs. In row a, $\langle 0|\hat{\mu}|1\rangle = 0.0223$ a.u. and $\langle 1|\hat{\mu}|2\rangle = 0.00446$ a.u. In row b, $\langle 0|\hat{\mu}|1\rangle = \langle 1|\hat{\mu}|2\rangle = 0.0223$ a.u. In row c, $\langle 0|\hat{\mu}|1\rangle = 0.00446$ a.u. and $\langle 1|\hat{\mu}|2\rangle = 0.0223$ a.u. These coupling values approximate those typically found in real systems. The value of 0.0223 a.u. corresponds to that of the real HF 0, 0 – 1, 1 coupling.

In the upper portion of each section of Fig. 6, the quasienergies of the three-level system have been depicted. The energy scale for these graphs is arbitrary since the topography of the quasienergies is what is important here. The unperturbed state most closely associated with a particular quasienergy state is used as a label for that QES. At each closest approach (avoided crossing) of a pair of quasienergies, the corresponding QES's "exchange" labels, i.e., they take on the unperturbed character of the other state. By noting which two unperturbed states are involved in the exchange, one can assign a mechanism to the corresponding peaks in the transition probability spectrum. Following is a summary of those mechanisms for each section of Fig. 6:

Column A: $|E_2 - E_1| = |E_1 - E_0|$

Row a: $V_{01} > V_{12}$—"Normal Autler–Townes splitting"

This case gives rise to the normally observed Autler–Townes splitting. There exists a large 0–1 interaction. Symmetrically distributed on either side of this peak are induced two-photon peaks due to the resonance between state 1 and 2. Since the induced two-photon peaks come from transitions out of state 1, the 0–1 transition drops. This leads to the hole-burning effect in the 0–1 transition at precisely the locations of the 0–2 transitions.

Row b: $V_{01} = V_{12}$—"Symmetric S hump"

Here again there is a large 0–1 transition. At the same frequency, however, there is a 1–2 interaction of equal magnitude. The 0–2 transition, which arises from these interactions, is narrower than the 0–1 transition present. Therefore, there is a 0–2 transition burning a hole in the center of the broader 0–1 peak. This gives rise to a 0–1 transition which has the appearance of being split.

Row c: $V_{01} < V_{12}$—"Inverted Autler–Townes splitting"

The primary interaction in this case is the coupling between the states 1 and 2. As can be seen from the diagram, there are a pair of 0–1 interactions symmetrically placed about the center of the 1–2 interaction. Since the upper two states are strongly coupled, wherever there is a one-photon transition, a two-photon transition will be induced. This causes the 0–1 peaks to be reduced in intensity and the 0–2 peaks to appear under the one-photon transitions.

Column B: $|E_2 - E_1| < |E_1 - E_0|$,

Row a: $V_{01} > V_{12}$ "Asymmetric Autler–Townes splitting".

The main feature in this spectrum is a large 0–1 transition peak. The two-photon peaks arise from two different mechanisms. The higher frequency peak comes from a direct 0–2 transition. A hole is burnt in the 0–1 peak at this location due to the shared initial state. The lower frequency peak is an induced transition due to the strong 0–1 transition followed by 1–2 coupling. Again, a hole is burnt in the 0–1 peak, but in this case it is due to the continuation of some of the model molecular systems through state 1 on to state 2.

Row b: $V_{01} = V_{12}$ "S-hump"

Again there is a large 0–1 transition and a 0–2 transition downfield from it. It is the effect of the 0–2 transition on the 0–1 peak which is of interest here. On the low frequency side of the 0–2 peak, the significant 1–2 coupling causes induced enhancement of the 0–1 transition from a $0 \rightarrow 2 \rightarrow 1$ emission process. On the high frequency side, the 0–1 peak is depleted by competition with the 0–2 peak for the initial state population. The intensity and location of the 0–2 transition are affected a small amount by these interactions. Taken all together, these effects lead to a pronounced S hump in the 0–1 transition.

Row c: $V_{01} < V_{12}$ "Induced transitions"

Here, there are independent 0–1 and 0–2 transitions. The strong 1–2 coupling, however, causes induced peaks to appear under those already present. Under the 0–2 peak there is an induced 0–1 transition from a $0 \rightarrow 2 \rightarrow 1$ emission process. Under the 0–1 peak there is an induced 0–2 transition from a $0 \rightarrow 1 \rightarrow 2$ continuation process. Both primary peaks are somewhat reduced in intensity by their participation in the creation of the induced peaks. The induced transitions, on the other hand, are less intense than the primary peaks, due to the more involved process leading to their existence.

Each of the sections explained above represents a limiting case. As the parameters involved are changed, one may move from one case to another via gradual steps. The mechanisms of transitions in these intermediate cases are not as well defined and should not be referred to in absolute terms. However, by resorting to these six quasienergy diagrams (and the three less common cases), one can explain many of the features found in intense field, multiphoton spectra. Likewise, by examining the features found experimentally, one can obtain qualitative information about the relative coupling strengths and detunings of the levels involved.

[1](a) *Nonlinear Behavior of Molecules, Atoms, and Ions in Electric, Magnetic or Electromagnetic Fields*, edited by L. Neel (Elsevier, Amsterdam, 1979). (b) *Photoselective Chemistry: Advances in Chemical Physics*, edited by J. Jortner, R. D. Levine, and S. A. Rice (Wiley, New York, 1981), Vol. 47. (c) *Coherent Nonlinear Optics*, edited by M. S. Feld and V. S. Letokhov (Springer, New York, 1980).
[2]See, for example, *Multiphoton Processes*, edited by J. Eberly and P. Lambropoulos (Wiley, New York, 1978).
[3]See, for example, (a) N. Bloembergen and E. Yablonovitch, Phys. Today **31**, 23 (1978); (b) P. A. Schulz, Aa. S. Suadbo, D. J. Krajnovich, H. S. Kwok, Y. R. Shen, and Y. T. Lee, Annu. Rev. Phys. Chem. **30**, 311 (1979).
[4]See, for example, R. W. Falcone, W. R. Green, J. C. White, J. F. Young, and S. E. Harris, Phys. Rev. A **15**, 1333 (1976); N. M. Kroll, and K. M. Watson, *ibid.* **13**, 1018 (1976); J. M. Yuan, J. R. Liang, and T. F. George, J. Chem. Phys. **66**, 1107 (1977); S. Yeh and P. R. Berman, Phys. Rev. A **19**, 1106 (1979).
[5]See, for example, T. F. George, J. Phys. Chem. **86**, 10 (1982); A. E. Orel and W. H. Miller, J. Chem. Phys. **70**, 990 (1979).
[6](a) P. Gozel and H. Van den Bergh, J. Chem. Phys. **74**, 1724 (1981); (b) R. Duperrex and H. Van den Bergh, *ibid.* **73**, 585 (1980).
[7]See, for example, H. J. Beyer and K. J. Kollath, J. Phys. B **10**, L5 (1977), and references therein.
[8]J. H. Shirley, Phys. Rev. B **138**, 979 (1965).
[9](a) D. R. Dion and J. O. Hirschfelder, Adv. Chem. Phys. **35**, 265 (1976), and references therein; (b) J. V. Moloney and W. J. Meath, Mol. Phys. **30**, 171 (1975); **31**, 1537 (1976).
[10](a) S. I. Chu and W. P. Reinhardt, Phys. Rev. Lett. **39**, 1195 (1977); (b) S. I. Chu, Chem. Phys. Lett. **54**, 367 (1978).
[11](a) S. I. Chu, Chem. Phys. Lett. **58**, 462 (1978); (b) **64**, 178 (1979).
[12]See, for example, *Proceedings of the* 1977 *Sanibel Workshop on Complex Scaling*, Int. J. Quantum Chem. **14**, No. 4 (1978).
[13]J. V. Moloney and F. H. M. Faisal, J. Phys. B **12**, 2829 (1979).
[14]S. I. Chu, Chem. Phys. Lett. **70**, 205 (1980).
[15](a) S. C. Leasure and R. E. Wyatt, Opt. Eng. **19**, 46 (1980); (b) S. C. Leasure, K. F. Milfeld, and R. E. Wyatt, J. Chem. Phys. **74**, 6197 (1981).
[16]C. D. Cantrell, V. S. Letokhov, and A. A. Makorov, in *Coherent Nonlinear Optics*, edited by M. S. Feld and V. S. Letokhov (Springer, New York, 1980), p. 165.
[17]S. I. Chu, J. Chem. Phys. **75**, 2215 (1981).
[18]K. K. Datta and S. I. Chu (to be published).
[19](a) J. V. Moloney and W. J. Meath, Mol. Phys. **35**, 1163 (1978); (b) J. V. Moloney and W. J. Meath, J. Phys. B **11**, 2641 (1978).
[20](a) R. B. Walker and R. K. Preston, J. Chem. Phys. **67**, 2017 (1977); (b) S. C. Leasure, K. F. Milfeld, and R. E. Wyatt, *ibid.* **74**, 6197 (1981).
[21]J. A. C. Gallas, Phys. Rev. A **21**, 1829 (1980).
[22]See, for example, I. Schek and J. Jortner, Chem. Phys. Lett. **63**, 5 (1979).
[23]See, for example, (a) S. H. Autler and C. H. Townes, Phys. Rev. **100**, 703 (1955); (b) J. V. Moloney and F. H. M. Faisal, Opt. Commun. **28**, 62 (1979).
[24]See, for example, (a) J. R. Ackerhalt and H. W. Galbraith, J. Chem. Phys. **69**, 1200 (1978); (b) Ref. 1(c).
[25]See, for example, (a) A. Javan, Phys. Rev. **107**, 1579 (1957); (b) J. Ackerhalt, J. Eberly, and B. Shore, Phys. Rev. A **19**, 248 (1979); (c) L. Kancheva, D. Pushkarov, and S. Rashev, J. Phys. B **14**, 573 (1981).
[26]In actual practice, the diagonalization of the Floquet matrix was performed in two steps. The sub-block A in Fig. 1 was prediagonalized to give transition probabilities between the dc-shifted levels of HF.